Supplementary Materials for

A global urban heat island intensity dataset: generation, comparison, and analysis

Qiquan Yang [a, b, c], Yi Xu [a, *], TC Chakraborty [d], Meng Du [e], Ting Hu [e], Ling Zhang [f], Yue Liu [g], Rui Yao [h], Jie Yang [h], Shurui Chen [b], Changjiang Xiao [b, c], Renrui Liu [a], Mingjie Zhang [a], Rui Chen [a]

[a] State Key Laboratory of Lunar and Planetary Sciences, Macau University of Science and Technology, Macau, China
[b] College of Surveying & Geo-Informatics, Tongji University, Shanghai, 200092, China
[c] The Shanghai Key Laboratory of Space Mapping and Remote Sensing for Planetary Exploration, Tongji University, Shanghai, 200092, China
[d] Pacific Northwest National Laboratory, Richland, WA, USA
[e] School of Remote Sensing and Geomatics Engineering, Nanjing University of Information Science and Technology, Nanjing, 210044, China
[f] School of Earth Science and Geological Engineering, Sun Yat-sen University, Guangzhou, 510275, China
[g] Guangzhou Institute of Geography, Guangdong Academy of Sciences, Guangzhou, 510070, China
[h] School of Remote Sensing and Information Engineering, Wuhan University, Wuhan, 430079, China

* Corresponding author: Yi Xu (yixu@must.edu.mo)

This file includes：

Supplementary tables (Table S1 to S3)

Supplementary figures (Fig. S1 to S8)

Table S1. A summary of previous UHII studies in the eight representative cities

City	Reference	Temperature data	Time scale	Methods for calculating UHII	Major results about the estimated UHII
Singapore	Chakraborty et al. (2019)	MODIS LST products	2008-2017	Difference between urban areas and all non-urban land pixels within city boundaries	The average magnitude of the surface UHII during the day and at night reaches 2.15 °C and 0.49 °C, respectively.
	Chow et al. (2006)	Air temperature recorded by meteorological stations	2003-2004	Difference between urban areas (commercial, CBD) and rural reference data	Higher canopy UHII generally occurs during May–August with a maximum magnitude of ∼7 °C.
	Wong and Yu, 2005	Air temperature collected by a mobile datalogger	July, 2002	Difference between Central Business District (CBD) and well planted areas	The maximum magnitude of canopy UHII reaches 4.01°C.
Calcutta	Das et al. 2020	MODIS LST products (MOD11C1)	March-May, 2008-2017	Difference between urban areas and rural reference data	The summer surface UHII has an average magnitude of 1.5 °C during the day and 0.4 °C at night.
	Das et al. 2020	Air temperature derived from the ERA-interim reanalyzed datasets	March-May, 2008-2017	Difference between urban areas and rural areas extracted by a rectangle method	The estimated daily average canopy UHII is only 0.023 °C.
Riyadh	Alghamdi and Moore, 2015	Air temperature recorded by two weather stations	1985-2010	Difference between the urban station and the rural station	The average magnitude of the canopy UHII is of the order of 2.00 °C at night and less than 0.12 °C during the day.
	Sherafati et al. 2018	LST estimated from AVHRR and Landsat images	2011-2012	Difference between urban areas and surrounding classes (bare soil, vegetation and water body)	The nighttime magnitude of surface UHII is about 3.7 °C in summer and 3.5 °C in winter.
	Chakraborty et al. (2019)	MODIS LST products	2008-2017	Difference between urban areas and all non-urban land pixels within city boundaries	The mean magnitude of the surface UHII during the day and at night is 3.97 °C and 0.5 °C, respectively.
	Haddad et al. 2024	Air temperature recorded by weather stations and simulated by WRF model	Summer, 2018	Difference between urban areas and reference locations	The average magnitude of the summer canopy UHII is 1.5 °C, and the maximum daytime canopy UHII reaches 8.5 °C.
Albuquerque	Kenward et al. 2014	Air temperature recorded by meteorological stations	2004-2014	Difference between urban stations and rural stations	The most intense summer canopy UHII reaches 3.28 °C.
Paris	Sherafati et al. 2018	LST estimated from AVHRR and Landsat images	2011-2012	Difference between urban areas and surrounding classes (bare soil, vegetation and water body)	The magnitude of nighttime surface UHII is about 2.7 °C in summer and 3.0 °C in winter.
	Le et al. 2019	MODIS LST products	2006-2015	Difference between urban areas and rural areas	Daytime surface UHII varies between 0.92 °C and 6.92 °C, whereas nighttime surface UHII varies between 1.51 °C and 3.43 °C.
	Le et al. 2019	Air temperature measured by stations	2006-2015	Difference between urban areas and rural areas	The average monthly magnitude of the canopy UHII in July reaches 2.45 °C during the night, but only 0.14 °C during the day.
	Chakraborty et al. (2019)	MODIS LST products	2008-2017	Difference between urban areas and all non-urban land pixels within city boundaries	The mean magnitude of the surface UHII during the day and at night is 1.98 °C and 0.9 °C, respectively.
Dallas	Ramamurthy and Sangobanwo, 2016	Air temperature observed by weather stations	2005-2014	Difference between urban stations and rural stations identified by local climate zones	The summer canopy UHII varies between 0.05°C and 1.6°C.
	Darby and Senff, 2007	Air temperature observed by weather conditions	Summer, 2000-2006	Difference between urban stations and rural stations	The canopy UHII varies from 1.5 °C to 2.0 °C during nighttime and is about 1.0 °C during daytime.
Edmonton	Ejiagha et al. 2022	MODIS monthly LST products (MOD11C3)	2001-2020	Difference between urban areas and rural areas (an equal-area buffer adjacent urban areas)	The annual daytime and nighttime surface UHIIs range from 0.19 to 0.39 °C and 0.47 to 0.51 °C, respectively.
Harbin	Liao et al. 2022	MODIS and TRIMS LST products	2009 and 2019	Difference between urban areas and rural areas (a buffer zone with a radius of 10 km)	The daytime surface UHII is highest in summer and lowest in winter, while the nighttime surface UHII is lowest in summer and highest in winter.
	Liu et al. 2020	Landsat 8	October, 2014	Difference between built-up and other non-built-up land covers	The estimated surface UHII is 0.0453 K.
	Wang et al. 2023	Universal thermal climate index	2018	Difference between urban areas and rural buffers (15 km outside the urban boundary)	The summer UHII is 3.57 °C during the day and 3.63 °C at night.

Table S2. A summary of global-scale studies on the average magnitude of UHII

Reference	Statistic	Time scale	Method	Period	Magnitude of UHII (ºC)							
					I_{Mod1}	I_{Myd1}	I_{Mod2}	I_{Myd2}	I_{SMod2}	I_{SMyd1}	I_{AMod2}	I_{SAT}
Chakraborty and Lee, 2019	7374 cities (mean ± std)	2001-2017	Simplified urban extent (SUE) method	Ann day			0.71 ± 0.82	1.00 ± 1.04				
				Ann night			0.59 ± 0.44	0.51 ± 0.44				
				Sum day			1.12 ± 1.19	1.44 ± 1.42				
				Sum night			0.69 ± 0.46	0.57 ± 0.44				
				Win day			0.35 ± 0.59	0.53 ± 0.79				
				Win night			0.57 ± 0.54	0.50 ± 0.54				
Clinton and Gong, 2013	/ (mean ± std)	2010	Distance-based method (5 km)	Ann day			0.70 ± 1.40	0.90 ± 1.60				
				Ann night			0.60 ±0.90	0.60 ± 0.90				
			Distance-based method (10 km)	Ann day			1.00 ± 1.60	1.10 ± 1.80				
				Ann night			0.80 ± 1.00	0.70 ± 1.00				
Du et al. 2021	336 cities (mean ± std)	2012	Distance-based method (1.5-10 km)	Ann day		1.7 ± 1.5						0.6 ± 1.3
				Ann night		1.1 ± 0.8						0.8 ± 1.4
Peng et al. 2012	419 cities (mean ± std)	2003-2008	Equal-area (EA) method	Ann day				1.5 ± 1.2				
				Ann night				1.1 ± 0.5				
				Sum day				1.9 ± 1.5				
				Sum night				1.0 ± 0.5				
				Win day				1.1 ± 1.2				
				Win night				1.0 ± 0.7				
Li et al. 2022	1112 cities (mean)	2018	MEA method	Ann day			1.73					
				Ann night			1.22					
Si et al. 2022	1711 cities (mean)	2003-2019	Dynamic urban-extent (DEA) method	Ann day			1.32					
				Ann night			1.09					
				Sum day			1.98					
				Sum night			1.05					
				Win day			0.76					
				Win night			1.10					

Table S3. A summary of global-scale studies on the inter-annual trend of UHII

Reference	Statistic	Time scale	Method	Period	Trend of UHII (ºC/decade)							
					I_{Mod1}	I_{Myd1}	I_{Mod2}	I_{Myd2}	I_{SMod2}	I_{SMyd1}	I_{AMod2}	I_{SAT}
Du et al. 2023	5643 cities (mean ± se)	2003-2020	Distance-based method (10-100 km)	Ann day				0.19 ± 0.006				0.03 ± 0.002
				Ann night				0.06 ± 0.004				0.03 ± 0.002
Yao et al. 2019	397 cities (mean ± std)	2001-2017	Distance-based method (10-30 km)	Ann day			0.29 ± 0.41					
				Ann night			0.10 ± 0.23					
				Sum day			0.45 ± 0.56					
				Sum night			0.12 ± 0.29					
				Win day			0.08 ± 0.48					
				Win night			0.09 ± 0.34					
Chakraborty and Lee, 2019	7374 cities (mean ± std)	2003-2017	Simplified urban extent (SUE) method	Ann day			0.03 ± 0.02					
				Ann night			−0.00 ± 0.01					
Si et al. 2022	1711 cities (mean)	2003-2019	Dynamic urban-extent (DEA) method	Ann day			0.11					
				Ann night			0.07					
				Sum day			0.27					
				Sum night			0.09					
				Win day			−0.06					
				Win night			0.10					

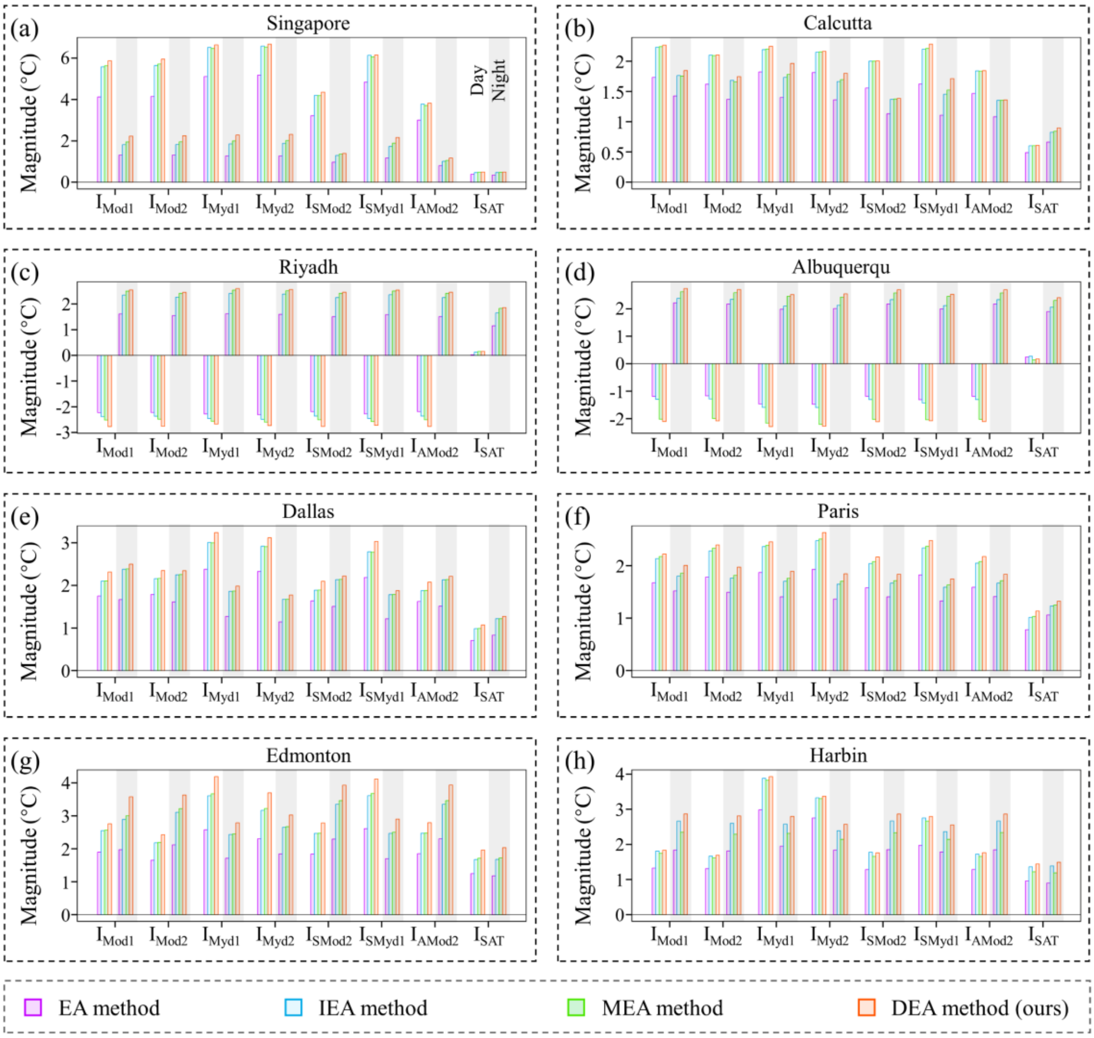

Fig. S1. The annual daytime and nighttime magnitudes of UHII, estimated by different methods (EA, IEA, MEA, and DEA), in eight representative cities during 2020. Please refer to the Methods section for detailed explanations of each method.

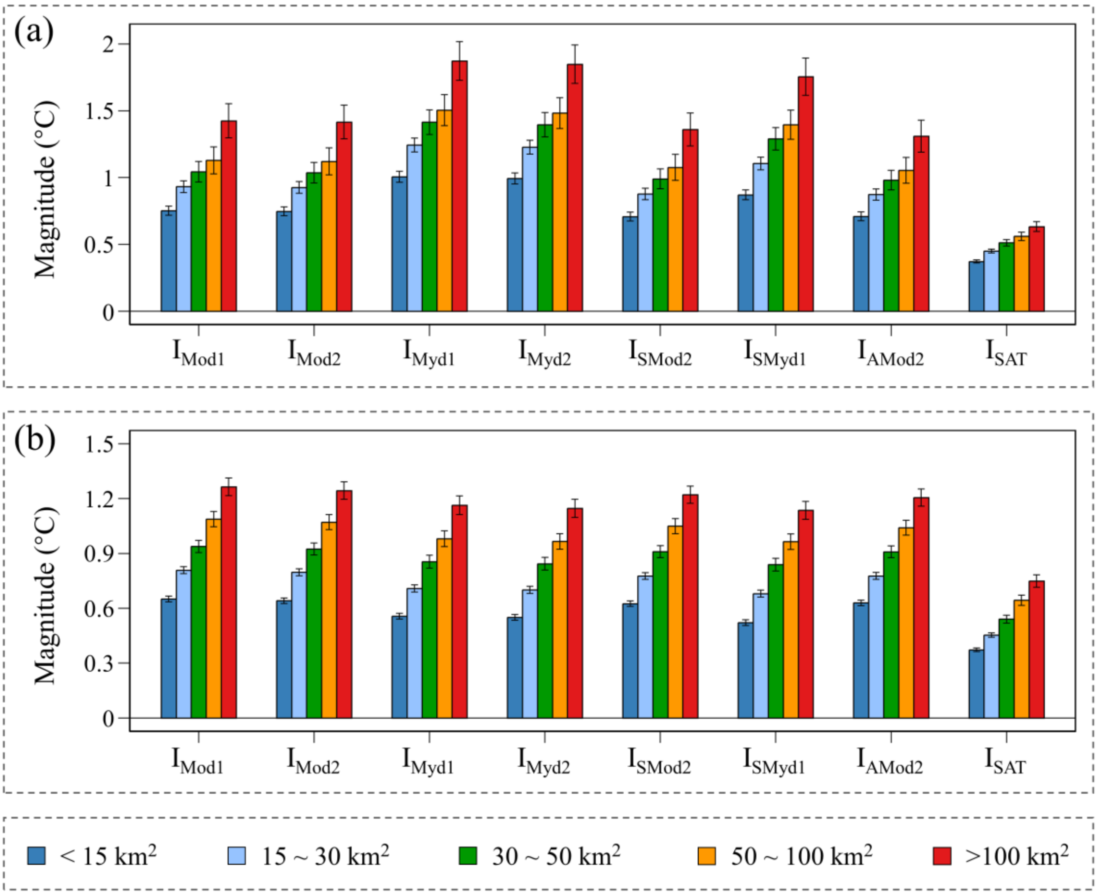

Fig. S2. Comparisons of the average magnitude of UHII among groups of different urban sizes. (a) Annual daytime results. (b) Annual nighttime results. Columns and error bars represent the averages and 95% confidence intervals, respectively. The magnitude is calculated as the average of UHII during 2003-2020.

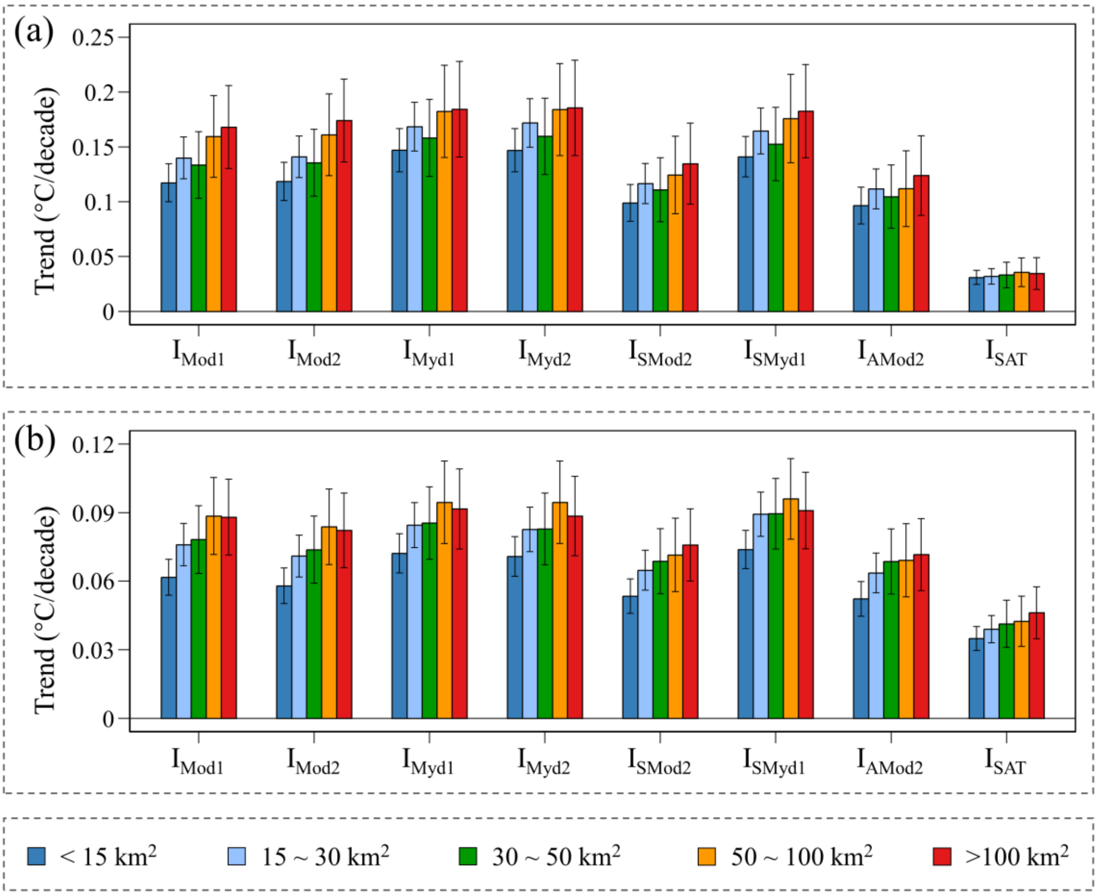

Fig. S3. Comparisons of the average trend of UHII among groups of different urban sizes. (a) Annual daytime results. (b) Annual nighttime results. Columns and error bars represent the averages and 95% confidence intervals, respectively. The trend denotes the change rate of UHII estimated based on year-by-year values during 2003-2020.

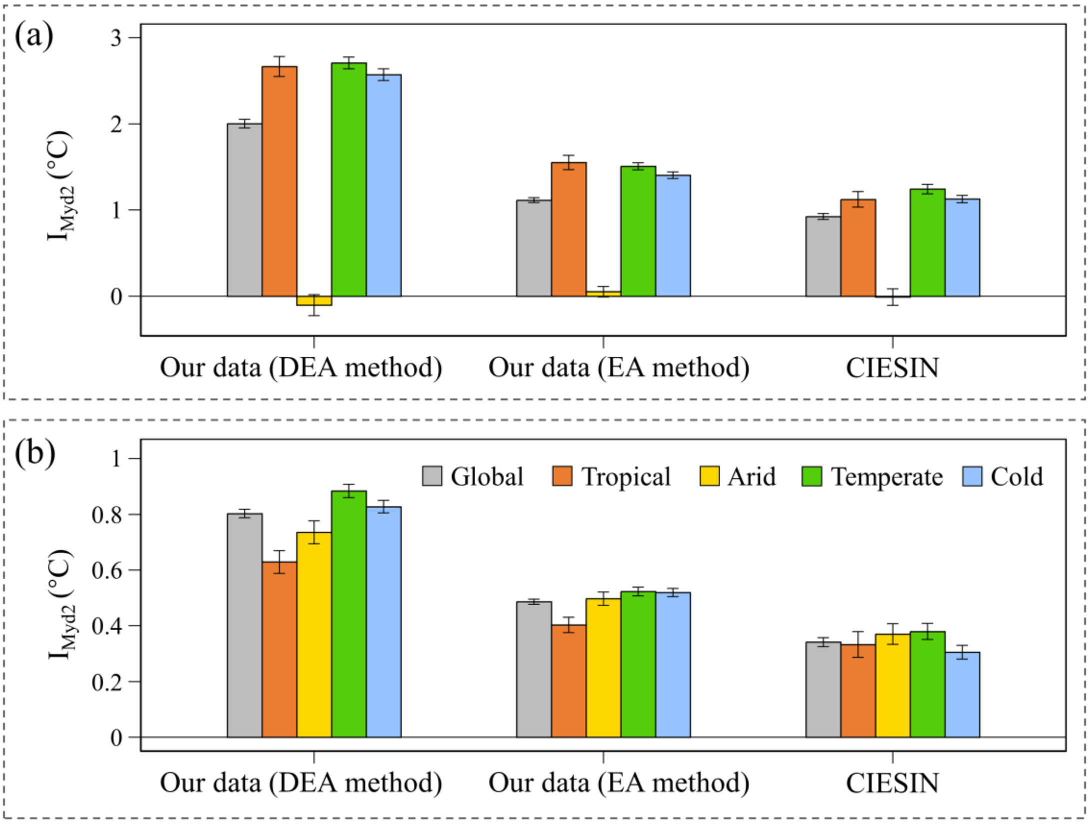

Fig. S4. Comparisons of surface UHII (I_{Myd2}) between ours and that released by CIESIN. (a) Summer daytime results during 2013. (a) Summer nighttime results during 2013. Columns and error bars in subplots represent the averages and 95% confidence intervals, respectively. The summer period here includes July-August for Northern Hemisphere cities and January-February for Southern Hemisphere cities (Center for International Earth Science Information Network - CIESIN - Columbia University 2016). The comparison analysis includes the largest 10,196 cities (the same number as in our dataset) from the CIESIN dataset. Please refer to the Methods section for detailed explanations of the EA and DEA methods.

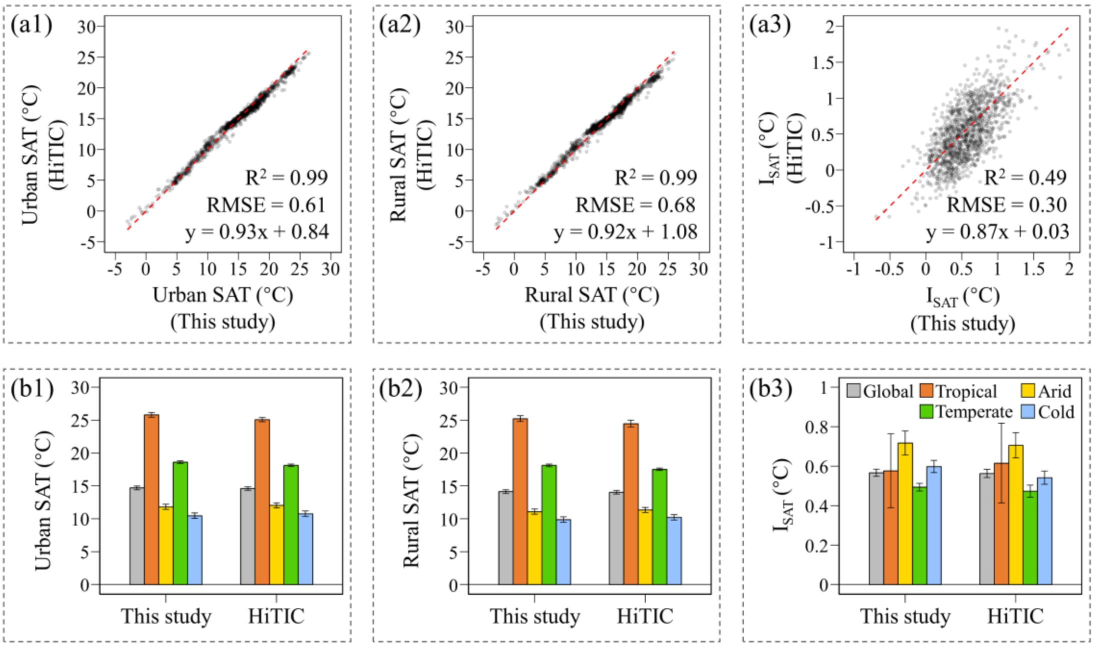

Fig. S5. Comparative analysis of surface air temperature (SAT) in urban and rural areas, as well as canopy UHII (I_{SAT}), across 1,241 Chinese cities. Columns and error bars in subplots (b1-b3) represent the averages and 95% confidence intervals, respectively. The SAT used in this study is provided by Yao et al. (2023), while the SAT for comparison purposes is derived from the HiTIC dataset published by Zhang et al. (2023). The HiTIC dataset only provides daily average SAT values for the mainland China. Therefore, to ensure a fair comparison, we averaged our daytime and nighttime SAT, as well as the corresponding I_{SAT}, represent their daily average values. This comparative analysis is based on the canopy UHII generated through our proposed DEA method for the year 2020.

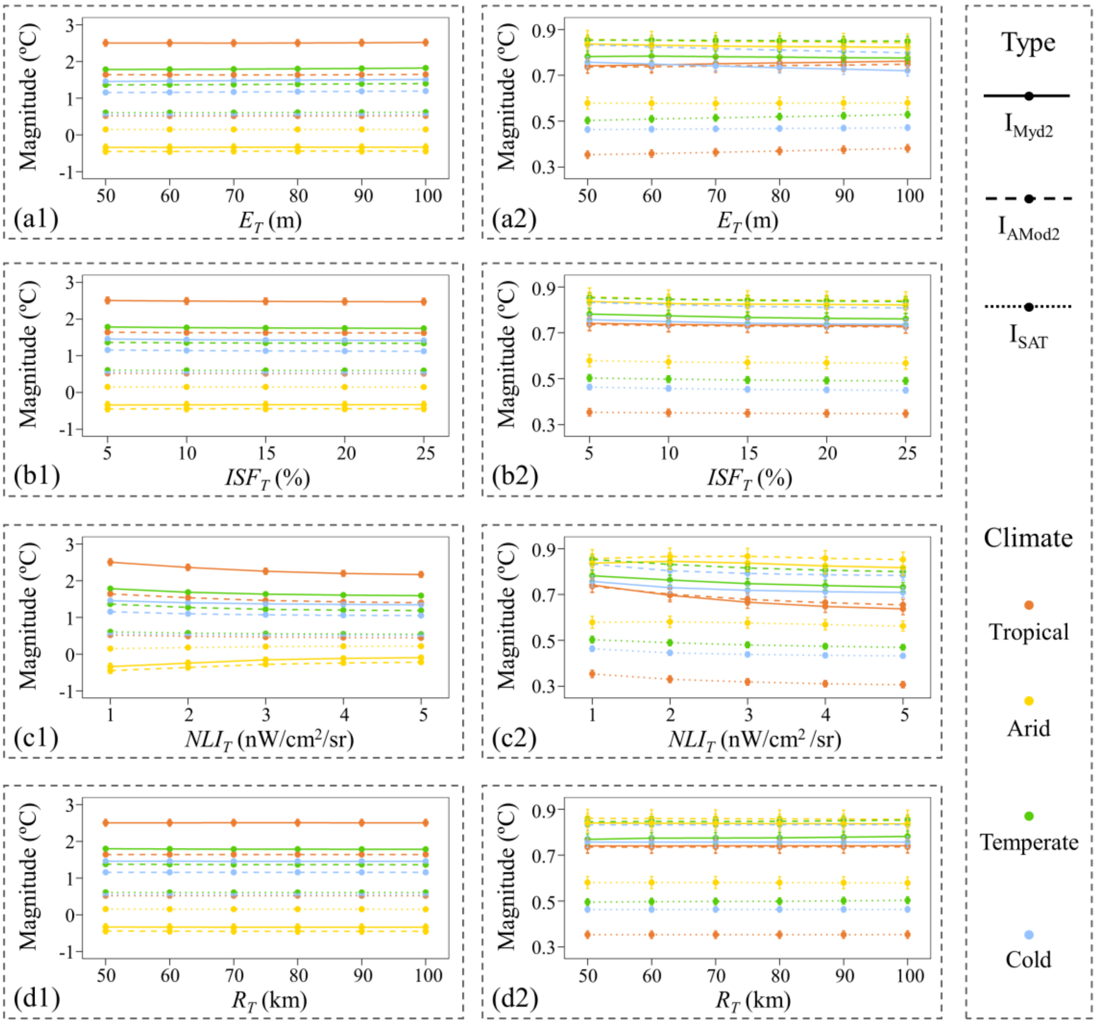

Fig. S6. Sensitivity of the average magnitude of UHII to the parameters in the DEA method across different climate zones. (a1-a2) E_T denotes the upper threshold of the difference between the elevation of pixels within the background reference area (BRA) and the median elevation of the urban area. (b1-b2) ISF_T represents the upper threshold of impervious surface fraction for pixels within the BRA. (c1-c2) NLI_T represents the upper threshold of nighttime light intensity for pixels within the BRA. (d1-d2) R_T is the upper threshold for the buffer radius when searching for suitable pixels of the BRA. Those on the left (a1-d1) represent annual daytime results and those on the right (a2-d2) represent annual nighttime results. Colored points and error bars represent the averages and 95% confidence intervals, respectively. The sensitivity analysis is based on estimated UHII using the DEA method for the year 2020. The sensitivity analysis was conducted for all eight UHII indicators, but only three (I_{Myd2}, I_{AMod2}, and I_{SAT}) are depicted in this figure due to the similarity of results among them. Please refer to Table 1 for detailed information regarding all the UHII indicators.

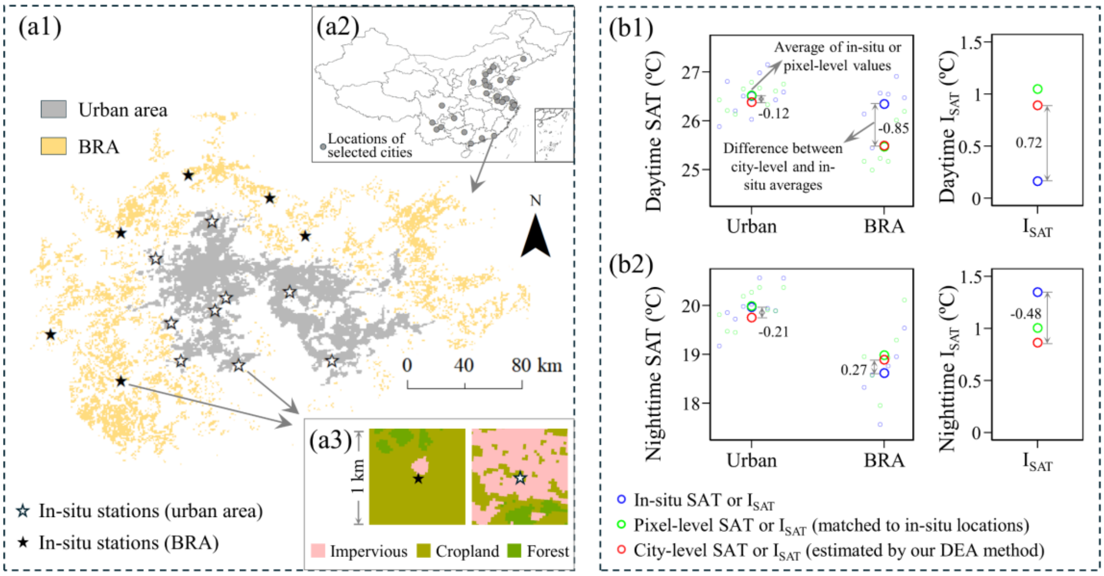

Fig. S7. Comparisons of surface air temperature (SAT) and canopy UHII (I_{SAT}) between that derived from the in-situ observations and that derived from the gridded data, taking the city of Pearl River Delta (PRD) as an example. (a1) Locations of in-situ meteorological stations in the largest Chinese city, PRD. (a2) Spatial distribution of the selected 30 Chinese cities, and each city is required to have at least one in-situ meteorological station both in the urban area and in the background reference area (BRA). (a3) Examples of land cover within the 1 km square (corresponding to the MODIS pixel) centered on the in-situ station. (b1-b2) Comparisons of SAT or I_{SAT} between that derived from the in-situ observations and that derived from the gridded data in the city of PRD. The in-situ SAT is derived from the China Meteorological Data Centre, and the pixel-level or city-level SAT is extracted from the gridded data provided by Yao et al (2023). The pixel-level SAT refers to the average gridded SAT of pixels at the locations of in-situ meteorological stations within the urban area or the BRA. The city-level SAT refers to the average gridded SAT across all available pixels within the urban area or the BRA.

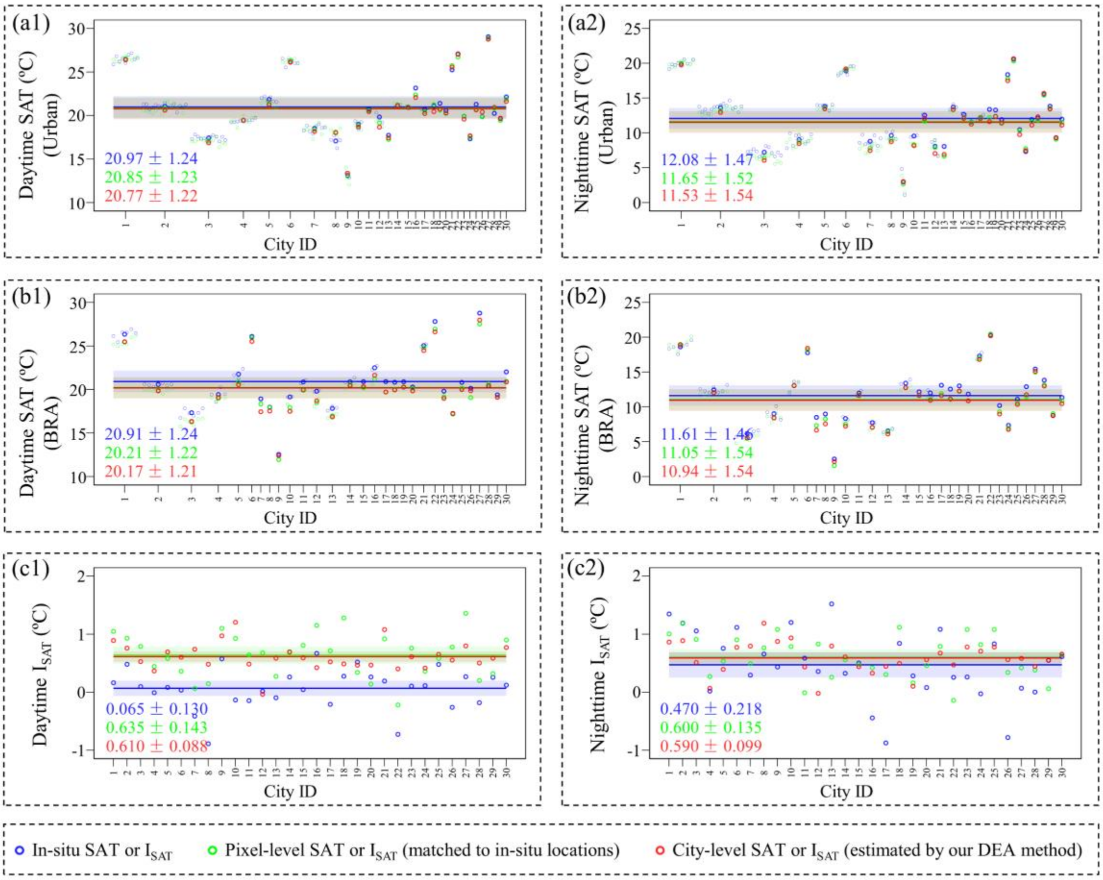

Fig. S8. Comparisons of surface air temperature (SAT) and canopy UHII (I_{SAT}) between that derived from the in-situ observations and that derived from the gridded data across 30 Chinese cities. The in-situ SAT is derived from the China Meteorological Data Centre, and the pixel-level or city-level SAT is extracted from the gridded data provided by Yao et al (2023). The pixel-level SAT refers to the average gridded SAT of pixels at the locations of in-situ meteorological stations within the urban area or the background reference area (BRA). The city-level SAT refers to the average gridded SAT across all available pixels within the urban area or the BRA. The colored horizontal lines and corresponding shaded areas indicate the mean and 95% confidence intervals for all cities, whose specific values are also placed in the lower left corner of each subplot. The locations of the 30 Chinese cities are presented in Fig. S7.

Reference

Alghamdi, A. S., & Moore, T. W. (2015). Detecting temporal changes in Riyadh's urban heat island. *Applied Geography*, 1(4), 312-325.

Chakraborty, T., Hsu, A., Manya, D., & Sheriff, G. (2019). Disproportionately higher exposure to urban heat in lower-income neighborhoods: a multi-city perspective. *Environmental Research Letters*, 14(10), 105003.

Chakraborty, T., & Lee, X. (2019). A simplified urban-extent algorithm to characterize surface urban heat islands on a global scale and examine vegetation control on their spatiotemporal variability. *International Journal of Applied Earth Observation and Geoinformation*, 74, 269-280

Center for International Earth Science Information Network - CIESIN - Columbia University (2016). Global Urban Heat Island (UHI) Data Set, 2013. In. Palisades, New York: NASA Socioeconomic Data and Applications Center (SEDAC)

Chow, W. T., & Roth, M. (2006). Temporal dynamics of the urban heat island of Singapore. *International Journal of climatology*, 26(15), 2243.

Clinton, N., & Gong, P. (2013). MODIS detected surface urban heat islands and sinks: Global locations and controls. *Remote Sensing of Environment*, 134, 294-304

Das, P., Vamsi, K. S., & Zhenke, Z. (2020). Decadal variation of the land surface temperatures (LST) and urban heat island (UHI) over Kolkata City projected using MODIS and ERA-interim DataSets. *Aerosol Science and Engineering*, 4, 200-209.

Darby, L. S., & Senff, C. J. (2007). Comparison of the urban heat island signatures of two Texas cities: Dallas and Houston. *In Seventh Symposium on the Urban Environment* (Expanded View).

Du, H., Zhan, W., Liu, Z., Li, J., Li, L., Lai, J., Miao, S., Huang, F., Wang, C., & Wang, C. (2021). Simultaneous investigation of surface and canopy urban heat islands over global cities. *ISPRS Journal of Photogrammetry and Remote Sensing*, 181, 67-83

Du, H., Zhan, W., Voogt, J., Bechtel, B., Chakraborty, T.C., Liu, Z., Hu, L., Wang, Z., Li, J., & Fu, P. (2023). Contrasting trends and drivers of global surface and canopy urban heat islands. *Geophysical Research Letters*, 50, e2023GL104661

Ejiagha, I. R., Ahmed, M. R., Dewan, A., Gupta, A., Rangelova, E., & Hassan, Q. K. (2022). Urban warming of the two most populated cities in the Canadian Province of Alberta, and its influencing factors. *Sensors*, 22(8), 2894.

Haddad, S., Zhang, W., Paolini, R., Gao, K., Altheeb, M., Al Mogirah, A., Moammar, A., Hong, T., Khan, A., Cartalis, C., Polydoros, A., & Santamouris, M. (2024). Quantifying the energy impact of heat mitigation technologies at the urban scale. *Nature Cities*, 1(1), 62-72.

Kenward, A., Yawitz, D., Sanford, T., & Wang, R. (2014). Hot and Getting Hotter: Heat Islands Cooking US Cities. *Climate Central*, 20.

Le Roy, B., Lemonsu, A., Kounkoud-arnaud, R., Brion, D., & Masson, V. (2019). Long time series spatialized data for urban climatological studies: a case study of Paris, France. *International Journal of Climatology*, 40(7), 3567-3584.

Liao, Y., Shen, X., Zhou, J., Ma, J., Zhang, X., Tang, W., Chen, Y., Ding, L., & Wang, Z. (2022). Surface urban heat island detected by all-weather satellite land surface temperature. *Science of The Total Environment*, 811, 151405.

Liu, F., Zhang, X., Murayama, Y., & Morimoto, T. (2020). Impacts of land cover/use on the urban thermal environment: a comparative study of 10 megacities in China. *Remote Sensing*, 12(2), 307.

Peng, S., Piao, S., Ciais, P., Friedlingstein, P., Ottle, C., Bréon, F.-M., Nan, H., Zhou, L., & Myneni, R.B. (2012). Surface urban heat island across 419 global big cities. *Environmental Science & Technology*, 46, 696-703

Ramamurthy, P., & Sangobanwo, M. (2016). Inter-annual variability in urban heat island intensity over 10 major cities in the United States. *Sustainable Cities and Society*, 26, 65-75.

Si, M., Li, Z.-L., Nerry, F., Tang, B.-H., Leng, P., Wu, H., Zhang, X., & Shang, G. (2022). Spatiotemporal pattern and long-term trend of global surface urban heat islands characterized by dynamic urban-extent method and MODIS data. *ISPRS Journal of Photogrammetry and Remote Sensing*, 183, 321-335

Sherafati, S., Saradjian, M. R., & Rabbani, A. (2018). Assessment of surface urban heat island in three cities surrounded by different types of land-cover using satellite images. *Journal of the Indian Society of Remote Sensing*, 46, 1013-1022.

Wang, C., Zhan, W., Li, L., Wang, S., Wang, C., Miao, S., Du, H., Jiang, L., & Jiang, S. (2023). Urban heat islands characterized by six thermal indicators. *Building and Environment*, 244, 110820.

Wong, N. H., & Yu, C. (2005). Study of green areas and urban heat island in a tropical city. *Habitat international*, 29(3), 547-558.

Yao, R., Wang, L., Huang, X., Cao, Q., Wei, J., He, P., Wang, S., & Wang, L. (2023). Global seamless and high-resolution temperature dataset (GSHTD), 2001–2020. *Remote Sensing of Environment*, 286, 113422

Yao, R., Wang, L., Huang, X., Gong, W., & Xia, X. (2019). Greening in rural areas increases the surface urban heat island intensity. *Geophysical Research Letters*, 46, 2204-2212

Zhang, H., Luo, M., Zhao, Y., Lin, L., Ge, E., Yang, Y., Ning, G., Cong, J., Zeng, Z., & Gui, K. (2023). HiTIC-Monthly: a monthly high spatial resolution (1 km) human thermal index collection over China during 2003–2020. *Earth System Science Data*, 15, 359-381